

Can the Frequency of Blocking Be Described by a Red Noise Process?

GIACOMO MASATO, BRIAN J. HOSKINS, AND TIM J. WOOLLINGS

Department of Meteorology, University of Reading, Reading, United Kingdom

(Manuscript received 30 July 2008, in final form 26 December 2008)

ABSTRACT

The frequency of persistent atmospheric blocking events in the 40-yr ECMWF Re-Analysis (ERA-40) is compared with the blocking frequency produced by a simple first-order Markov model designed to predict the time evolution of a blocking index [defined by the meridional contrast of potential temperature on the 2-PVU surface ($1 \text{ PVU} \equiv 1 \times 10^{-6} \text{ K m}^2 \text{ kg}^{-1} \text{ s}^{-1}$)]. With the observed spatial coherence built into the model, it is able to reproduce the main regions of blocking occurrence and the frequencies of sector blocking very well. This underlines the importance of the climatological background flow in determining the locations of high blocking occurrence as being the regions where the mean midlatitude meridional potential vorticity (PV) gradient is weak. However, when only persistent blocking episodes are considered, the model is unable to simulate the observed frequencies. It is proposed that this persistence beyond that given by a red noise model is due to the self-sustaining nature of the blocking phenomenon.

1. Introduction

It is evident that atmospheric blocking is an important phenomenon and that its understanding could greatly improve medium-range weather forecasts. Many studies have been performed stressing the characteristic persistence of blocking, starting from Rex (1950a, b). It is often implicitly assumed that blocking is a distinct phenomenon with characteristics and dynamics that are in some way different from other synoptic-scale anticyclones. But is this true, or is the distinction between a block and a synoptic ridge purely semantic? The aim of this note is to address this question by comparing observations of blocking with the output from a first-order Markov model, as suggested by Tyrlis and Hoskins (2008a, hereafter TH08a). Such a model is the simplest possible statistical red noise model, and yet many of the characteristics of transient synoptic-scale eddies can be well modeled by such a process (Branstator 1995; Whitaker and Sardeshmukh 1998). If the observed occurrence of blocking were also consistent with such a simple model, then not only would the distinction appear to be purely semantic, but also the potential that

the predictability of blocking could exceed that of a Markov process would be at best very limited.

This question has been examined by other studies. For instance, Dole (1986) analyzed 14 yr of winter 500-mb geopotential height data by comparing the observations with a Markov model, finding that the positive anticyclonic anomalies seemed to be more persistent than both the negative cyclonic ones and red noise. Moreover, he found that a nonlinear development of this model simulated quite well the statistical characteristics of blocking persistence. Here this behavior will be investigated further, exploiting the potential vorticity (PV) diagnostic of blocking introduced by Pelly and Hoskins (2003, hereafter PH03). This diagnostic involves a hierarchy of blocking indices that successively build in spatial and temporal constraints on the events classed as blocking. By using this hierarchy of indices, we are able to determine whether it is indeed the persistence of observed blocking that results in deviation from the behavior of the Markov model.

2. Data and methodology

The data used here come directly from TH08a. There a daily mean index B is calculated for each longitude following the method derived in PH03 using 40-yr European Centre for Medium-Range Weather Forecasts (ECMWF) Re-Analysis (ERA-40) reanalysis; B is calculated daily from 1 October 1957 to 31 December

Corresponding author address: Giacomo Masato, Department of Meteorology, University of Reading, Early Gate, Reading RG6 6BB, United Kingdom.
E-mail: swr07gm@rdg.ac.uk

2001. This study will be concentrating only on the winter periods.

Following PH03 and TH08a, the B index is a macro-scale measure of the strength of the meridional gradient of potential temperature θ on the isopotential vorticity surface with value of 2 PVU (also called the PV2 surface; $1 \text{ PVU} \equiv 1 \times 10^{-6} \text{ K m}^2 \text{ kg}^{-1} \text{ s}^{-1}$). This surface corresponds approximately to the tropopause, as in Hoskins et al. (1985). Here B is calculated (every 5° of longitude) as the difference of the average of θ for regions 15° of latitude on either side of a central latitude. This central latitude varies with longitude and follows the maximum of the smoothed transient eddy kinetic energy, which is an indication of the main track followed by synoptic systems. Whenever B takes positive values (θ higher on the poleward side), it is named local instantaneous blocking (LIB) and is taken as an indication of the possible presence of blocking for a particular point of longitude at a particular time. In addition, two more definitions have been created. The first puts a requirement on the spatial behavior, defining that sector blocking (SB) occurs in a sector 45° of longitude wide centered at the longitude of interest whenever LIB occurs at three consecutive points within it. The second places a requirement on the temporal coherence and defines a sector blocking episode (SBE) as the presence of SB at a given longitude for at least 5 consecutive days. These two definitions discriminate between a synoptic event and a full blocking event.

3. Results

The model constructed here has been developed in two stages that we will call the 1D and 2D models. The basic equation for the 1D model at day n ,

$$\Delta B_n = \phi(\Delta B_{n-1}) + \epsilon_n, \quad (1)$$

can be integrated to generate a time series for the deviation ΔB from the mean of the B index. The autoregressive parameter ϕ is the lag-1 autocorrelation in time calculated from the observations, and ϵ refers to the white noise variable (Wilks 2006, chapter 8). The amplitude of the noise term is chosen such that the variance of ΔB matches that of the observations, and ϵ and ϕ are calculated as independent of longitude (although they vary relatively little with it). For the model to fit the original data, it requires a climatological mean calculated from the observations at each point of longitude and then added to the ΔB series. To reduce the influence of a few extreme values, the median of the observations was chosen instead of the mean, although this has only a very small effect on the results. In the 1D

model, Eq. (1) is integrated at each longitude independently. Although the temporal correlations are well described by the model (not shown), the different time series are temporally independent of those at neighboring longitudes.

It is then necessary to build in the observed spatial coherence into the model. To do this, a 2D model has been constructed from the 1D model by applying a correlation matrix at each time step:

$$\Delta \mathbf{B}_n^* = \phi(\Delta \mathbf{B}_{n-1}) + \boldsymbol{\epsilon}_n, \quad (2)$$

$$\Delta \mathbf{B}_n = (\Delta \mathbf{B}_n^*) \mathbf{A}. \quad (3)$$

Here, $\Delta \mathbf{B}_n$ is a 1×72 column vector with 72 component elements (namely, 1 point every 5° of longitude), $\Delta \mathbf{B}_n^*$ is a vector containing intermediate values, and \mathbf{A} is a constant 72×72 matrix. The constant elements entered in \mathbf{A} were chosen empirically in the following manner. The first points on either side were calculated by using the autocorrelation in space derived from the observations. The second and third on either side were then chosen to ensure a spatial correlation structure similar to that of the observations. Therefore, each point in longitude is linked only to the three nearest points on either side, so that most of the off-diagonal elements in \mathbf{A} are zero. Note that the construction of the model means that the noise terms are also spatially correlated, so the model is structurally distinct from a standard multivariate Markov process. This is desirable, however, because much of the variability represented by the noise will be of at least synoptic scale and so will also be spatially correlated. Figure 1 shows the temporal and spatial correlation of the 2D model, which are both in good agreement with those from observations.

The longitudinal distributions of blocking given by the model are shown in Fig. 2. In addition to a well-simulated LIB frequency, there is also a striking agreement for the SB events. However, a significant gap between the observations and the model is present in the SBE frequency (Fig. 2, bottom). From these results it can be argued that the climatology of the gradient (\bar{B}) is pivotal for the model to perform well. Unless its variation with longitude is added to the time series, the model is completely unable to represent the blocking frequency seen in observations. This fact leads also to an important consequence: whenever the climatology of the blocking frequency is known—say, for example, in the winter season—then the general nature of the blocking occurrence for that particular season can be predicted. However, although the model has been refined and has given satisfactory results both for the LIB and the SB events, its representation is poor for the frequency of SBE, namely those events that persist longer than 5 days.

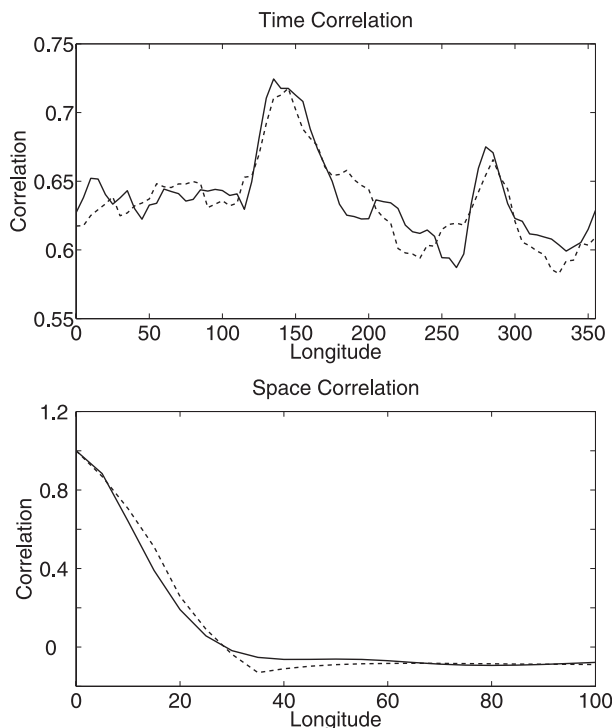


FIG. 1. 2D model. (top) Lag-1 autocorrelation in time of ΔB as a function of longitude. The solid line indicates the observations and the dashed line indicates the model. (bottom) Correlation of ΔB as a function of spatial lag (degrees of longitude) for the observations (solid) and the model (dashed).

One region of particular interest is the sector 200° – 270° E, where the statistical model significantly overestimates the LIB and SB (though not SBE) frequencies. Of interest in this regard is the skewness (third moment about the mean) and kurtosis (fourth moment about the mean) of the observed index, shown in Fig. 3. The former is a measure of the relative enhancement of the right- or left-hand tails (compared with a Gaussian distribution), whereas the latter indicates the extent to which the distribution is flattened. It is only in this band of longitude that both the skewness and kurtosis of the observations (Fig. 3, solid line) are well beyond the threshold fixed by the standard error (see the appendix). The negative skewness shows that positive values of B are underpopulated, so the model would be expected to overestimate blocking here. A high kurtosis instead indicates enhanced tails of the distribution and also indicates low occurrence of moderately large values (between the tails and the center of the distribution), and this is the most probable reason leading to the decrease in the blocking frequency for the observations. The impact of this on blocking frequencies is dependent on the location of the zero threshold for B with respect to the distribution [see Fig. 4a in TH08a, where the prob-

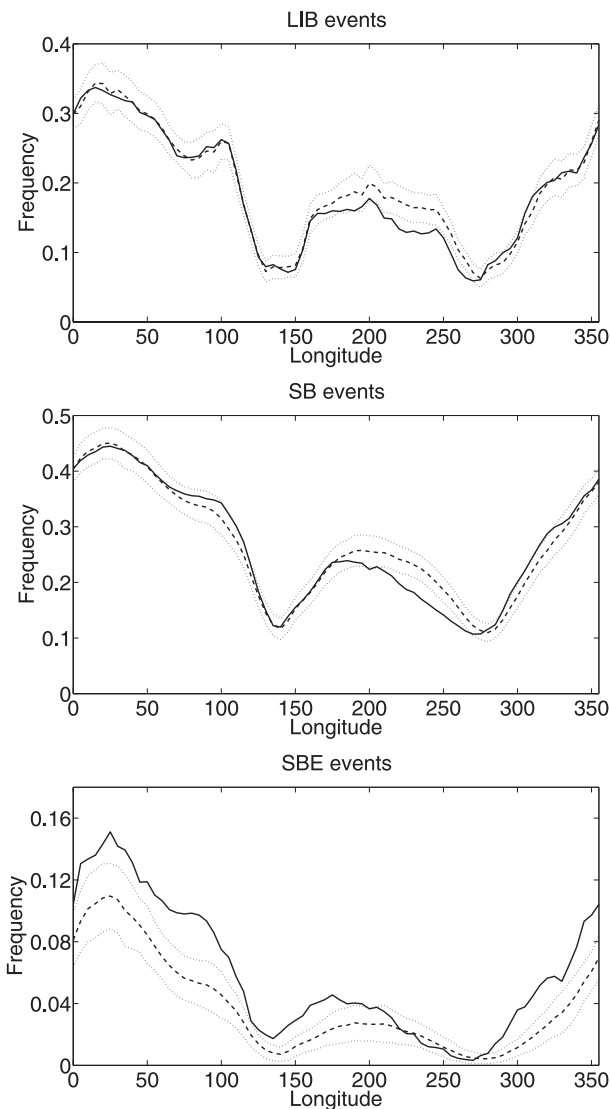


FIG. 2. Frequency of occurrence of (top) LIB, (middle) SB, and (bottom) SBE events as a function of longitude for the 2D model. The solid line is for the observations and the dashed line for the model. The dotted lines indicate the $\pm 2\sigma$ of 50 model runs.

ability density functions (PDFs) for the Pacific region are plotted]. Thus, again the mean value \bar{B} is seen to be very important. In general, there are several possible sources of non-Gaussian behavior, for example multiplicative noise (Sura et al. 2005) or truly nonlinear dynamics (Majda et al. 2008). In the conclusions we also discuss the possibility that this may arise from the particular low-frequency variability in this region.

The positive skewness in the region 30° – 110° E (Fig. 3) does not appear to lead to an underestimation by the model of LIB in the region. However it may contribute to the underestimation of SB and SBE in the eastern part of the region (Fig. 2).

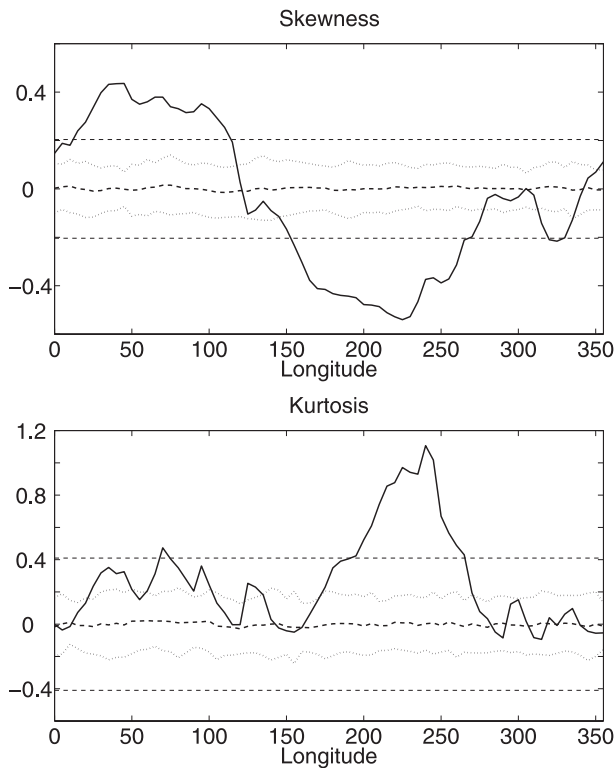


FIG. 3. (top) Skewness and (bottom) kurtosis of B as a function of longitude. The thick solid line is for the observations; the thick dashed line for the model with the error band ($\pm 2\sigma$) dotted. The thin dashed lines are the standard error values calculated using the formula in the appendix.

There has recently been interest in the occurrence of blocking-like events at higher latitudes (e.g., Schierz et al. 2004), and the frequencies of these have been found to be closely linked to the phase of the North Atlantic Oscillation (Woollings et al. 2008, hereafter W08). With this in mind, the statistical model has also been applied to higher northern latitudes, on the poleward side of the oceanic storm tracks, to determine whether the frequencies of occurrence of such events are consistent with a red noise process. As in W08, for high-latitude blocking, the central blocking latitude used in the definition of B has been changed to a line of latitude over the relevant Atlantic and Pacific regions: 55°N for the sector $290^{\circ}\text{--}330^{\circ}\text{E}$ and 45°N for $135^{\circ}\text{--}200^{\circ}\text{E}$. As seen in Fig. 4, both the observations and the model give a peak in frequency near 300°E over the North Atlantic. As before, the model significantly underestimates SBE frequency, confirming that the blocking events are more persistent than a red noise process would suggest. In the Pacific, east of the date line, the statistical model again overestimates the LIB frequency, as was the case for midlatitude blocking (Fig. 2).

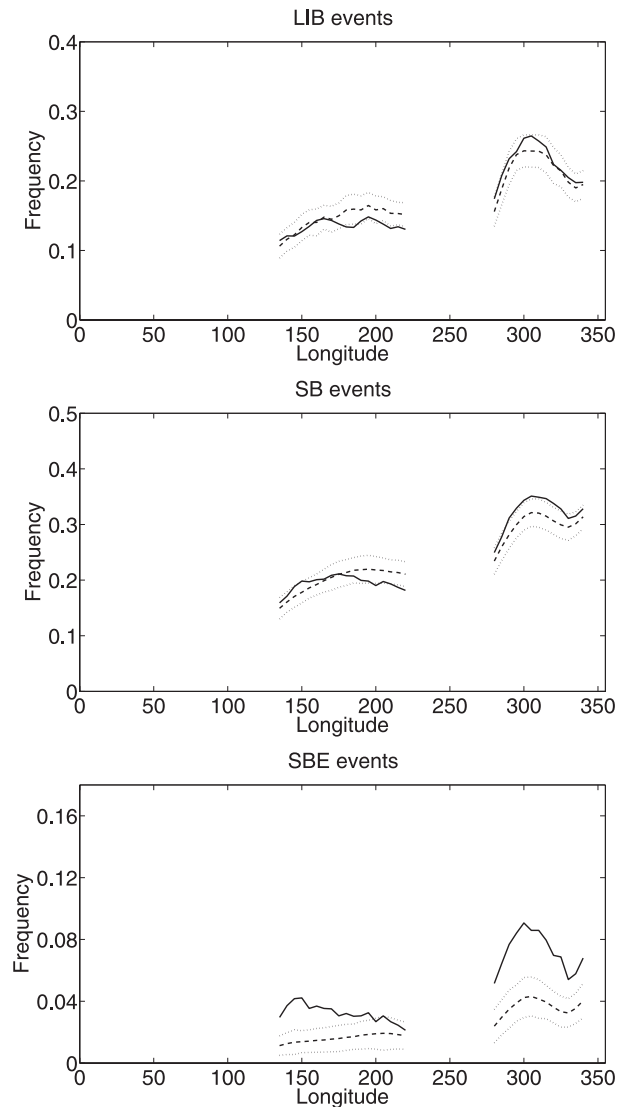


FIG. 4. Frequency of occurrence of (top) LIB, (middle) SB, and (bottom) SBE events as a function of longitude for the high-latitude blocking. The solid line indicates observations and the dashed line indicates the model. The dotted lines indicate $\pm 2\sigma$ for 50 model runs.

Finally, the persistence of SB events is examined using plots of the logarithm of the frequency of the events occurrence as a function of their duration (as in TH08a). In Fig. 5 the results are shown for three areas—Europe ($0^{\circ}\text{--}30^{\circ}\text{E}$), the Atlantic ($300^{\circ}\text{--}350^{\circ}\text{E}$), and the Pacific ($160^{\circ}\text{--}230^{\circ}\text{E}$)—by averaging the curves obtained for each point of longitude in the relevant region. The shallowing of the slope with increasing duration is evident for all the graphs, with the difference between the model and the observations being larger for longer-lasting events. This supports the hypothesis that dynamical processes lead to persistence beyond that given by a

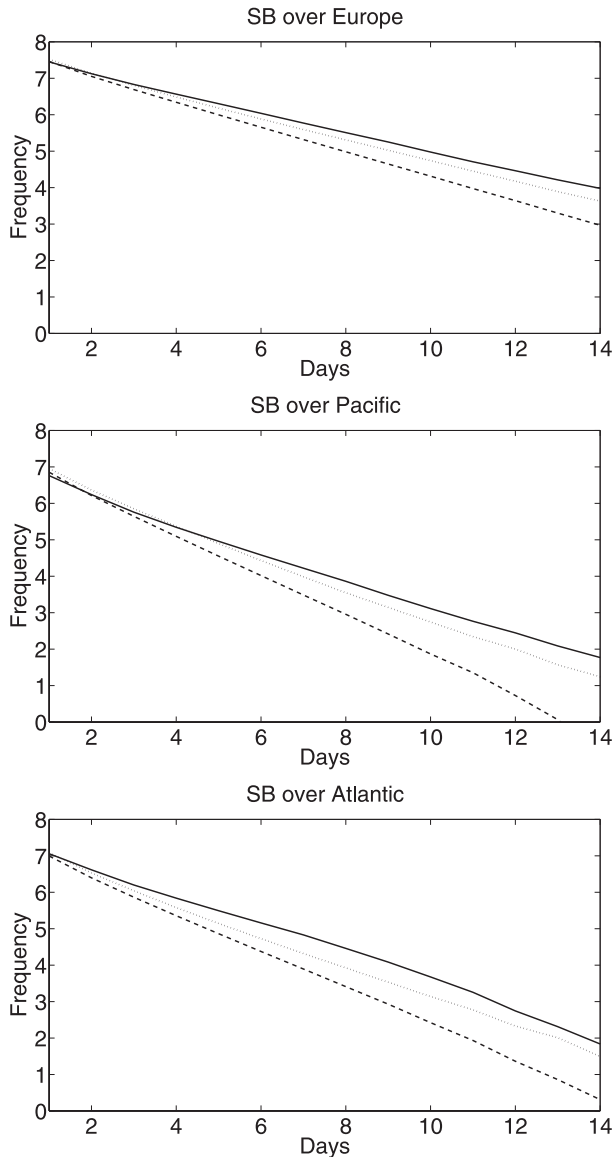


FIG. 5. The logarithm of the SB frequency as a function of the number of days persistence, averaged for (top) 0°–30°E (Europe), (middle) 160°–230°E (Pacific), and (bottom) 300°–350°E (Atlantic) sectors. The solid line is for the observations, the dashed line for the model, and the dotted line for the upper limit fixed by 2σ for 50 model runs.

red noise model. However, log–log plots show that blocks decay faster than would be given by any power law.

4. Conclusions

The main aim of this study is to examine the extent to which observed blocking frequency and persistence are consistent with a simple red noise model of statistical

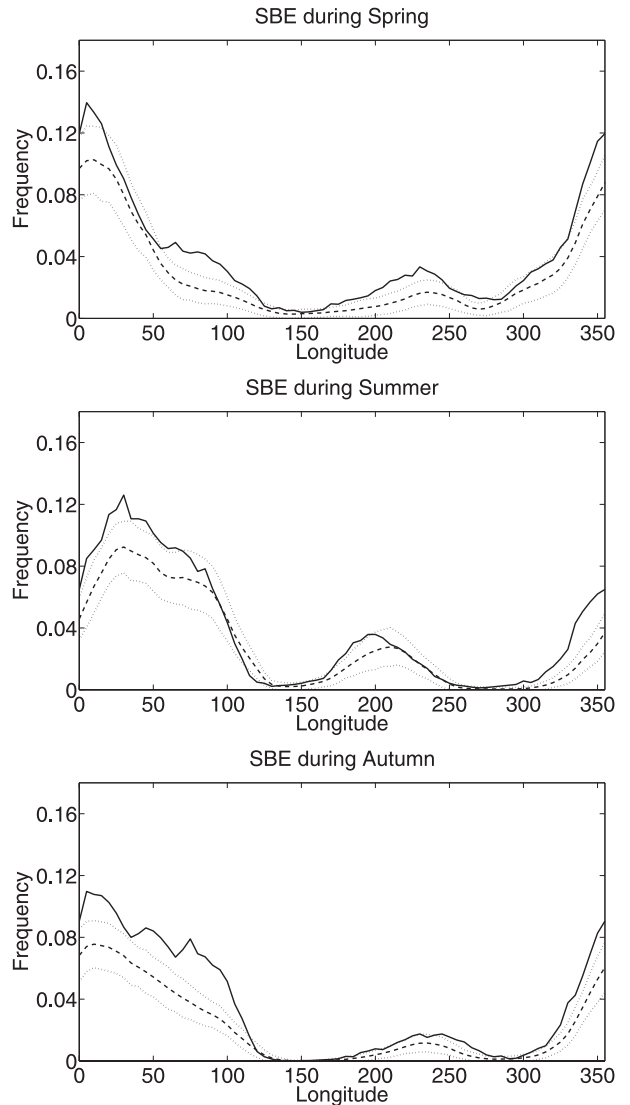


FIG. 6. Frequency of SBE for the (top) spring, (middle) summer, and (bottom) autumn periods as a function of longitude. The solid line is for the observations, the dashed line for the model, and the dotted line for the error band delimited by $\pm 2\sigma$.

variability. This study has been based on the perspective of blocking introduced by PH03. The first point to note is the remarkable ability of the model to describe the instantaneous measure of blocking frequency. This implies that blocking regions are strongly determined by the climatological mean flow, with blocking being much more present in the regions of the mean ridges (e.g., over Europe).

However, the model fails to capture the observed frequency of SBE where the definition of blocking has included persistence beyond the synoptic time-scale. Similar tests have been performed for the frequencies

of SBE during the other seasons, and Fig. 6 shows that underestimation occurs for all of them. The dependence on the different mean B values for the various seasons is also apparent. The discrepancy between model and observations confirms the results of Dole (1986) and TH08a with regard to the slower decay of longer-lived blocking. This also confirms that blocking is distinct from other more transient anticyclones, as the result for LIB shows that the occurrence of the latter is consistent with the Markov model. Such an enhanced persistence of blocking is in fact consistent with Rossby wave breaking and the cutting off of PV anomalies (Tyrlis and Hoskins 2008b) and with the eddy-straining feedback mechanism of Shutts (1983), as also described by the e -vector approach of Hoskins et al. (1983). Therefore, the fact that the Markov model underestimates the occurrence of blocking shows that there is potential for dynamical models to give more skillful forecasts.

The importance of the mean value of B in largely determining the likely occurrence of blocking raises a number of issues. It would be expected that low-frequency changes in the mean value of B as given, for example, by the Pacific decadal and Atlantic multi-decadal oscillations would, if used in the statistical model, give a better basis for the simulation of blocking occurrence. This notion could be extended to ENSO and to Pacific–North America (PNA) and North Atlantic Oscillation (NAO) variations, although it is probable that the minimum time scale considered for these should be greater than a season because at that time scale there can be an intimate relationship between recurrent blocking and the signatures of the patterns themselves, particularly in the case of the NAO (e.g., W08). The relative failure of the statistical model in the Pacific region seems to be linked to the large values of skewness and kurtosis there, which are not incorporated into the model, and these could be associated with the low-frequency variations in that region.

The dependence of blocking frequency on the mean value of B raises the intriguing and encouraging possibility that a climate model that has a good representation of the mean planetary waves but does not simulate blocking well could be used to infer the mean changes in blocking with, for example, enhanced greenhouse gases. For seasonal forecasting the intimate relationship between seasonal means and recurrent blocking may limit the ability to make such inferences.

Acknowledgments. We are grateful to Randall Dole, Mike Wallace, and the editor and reviewers for constructive feedback, which has been particularly useful.

We would also like to thank ECMWF for supplying the data.

APPENDIX

Standard Error

The standard error is calculated for the skewness and the kurtosis to determine whether their values are statistically significant. Following White (1980), significance bounds are estimated as $\pm 2SE$, where the standard error (SE) is given by

$$SE = \left(\frac{6}{N}\right)^{1/2}, \quad (\text{A1})$$

where N is the number of independent data values. Assuming that an independent sample is realized every 7 days, the 3991 days used here correspond to $N = 570$ independent samples. The choice of 7 days is justified as the e -folding parameter of the B index derived from the correlation in time. Therefore, from (A1), the error band is ± 0.205 .

For the kurtosis

$$SE = \left(\frac{24}{N}\right)^{1/2} \quad (\text{A2})$$

and the error band of ± 0.41 is found.

REFERENCES

- Branstator, G., 1995: Organization of storm-track anomalies by recurring low-frequency circulation anomalies. *J. Atmos. Sci.*, **52**, 207–226.
- Dole, R. M., 1986: Persistent anomalies of the extratropical Northern Hemisphere wintertime circulation: Structure. *Mon. Wea. Rev.*, **114**, 178–207.
- Hoskins, B. J., I. N. James, and G. H. White, 1983: The shape, propagation, and mean-flow interaction of large-scale weather systems. *J. Atmos. Sci.*, **40**, 1595–1612.
- , M. E. McIntyre, and A. W. Robertson, 1985: On the use and significance of isentropic potential vorticity maps. *Quart. J. Roy. Meteor. Soc.*, **111**, 877–946.
- Majda, A. J., C. Franzke, and B. Khouider, 2008: An applied mathematics perspective on stochastic modelling for climate. *Philos. Trans. Roy. Soc.*, **366**, 2429–2455.
- Pelly, J. L., and B. J. Hoskins, 2003: A new perspective on blocking. *J. Atmos. Sci.*, **60**, 743–755.
- Rex, D. F., 1950a: Blocking action in the middle troposphere and its effects upon regional climate. I. An aerological study of blocking action. *Tellus*, **2**, 196–211.
- , 1950b: Blocking action in the middle troposphere and its effects upon regional climate. II. The climatology of blocking action. *Tellus*, **2**, 275–301.
- Schwierz, C., M. Croci-Maspoli, and H. Davies, 2004: Perspicacious indicators of atmospheric blocking. *Geophys. Res. Lett.*, **31**, L06125, doi:10.1029/2003GL019341.

- Shutts, G. J., 1983: The propagation of eddies in diffluent jet streams: Eddy vorticity forcing of 'blocking' flow fields. *Quart. J. Roy. Meteor. Soc.*, **109**, 737–761.
- Sura, P., M. Newman, C. Penland, and P. Sardeshmukh, 2005: Multiplicative noise and non-Gaussianity: A paradigm for atmospheric regimes? *J. Atmos. Sci.*, **62**, 1391–1409.
- Tyrlis, E., and B. J. Hoskins, 2008a: Aspects of a Northern Hemisphere atmospheric blocking climatology. *J. Atmos. Sci.*, **65**, 1638–1652.
- , and —, 2008b: The morphology of Northern Hemisphere blocking. *J. Atmos. Sci.*, **65**, 1653–1665.
- Whitaker, J. S., and P. D. Sardeshmukh, 1998: A linear theory of extratropical synoptic eddy statistics. *J. Atmos. Sci.*, **55**, 237–258.
- White, G. H., 1980: Skewness, kurtosis, and extreme values of Northern Hemisphere geopotential heights. *Mon. Wea. Rev.*, **108**, 1446–1455.
- Wilks, S. D., 2006: *Statistical Methods in the Atmospheric Science*. Elsevier, 627 pp.
- Woollings, T. J., B. J. Hoskins, M. Blackburn, and P. Berrisford, 2008: A new Rossby wave-breaking interpretation of the North Atlantic Oscillation. *J. Atmos. Sci.*, **65**, 609–626.